ACS Photonics

Article

pubs.acs.org/journal/apchd5

Image Dipole Method for the Beaming of Plasmons from Point Sources

Di Zhu,[‡,⊥,†] Zhaogang Dong,[‡,†] Hong-Son Chu,[§] Yuriy A. Akimov,[§] and Joel K. W. Yang*[,‡,∥]

[‡]Institute of Materials Research and Engineering, A*STAR (Agency for Science, Technology and Research), 3 Research Link, 117602, Singapore

[§]Institute of High Performance Computing, A*STAR (Agency for Science, Technology and Research), 1 Fusionopolis Way, #16-16 Connexis, 138632, Singapore

[∥]Singapore University of Technology and Design, 20 Dover Drive, 138682, Singapore

Supporting Information

ABSTRACT: A point dipole source models the electrical excitation of surface plasmon polaritons (SPPs), and is promising as a compact source for the beaming of plasmons in optical nanocircuits. However, conventional design approaches rely on iterative numerical simulations to achieve beaming from dipole sources, and they consume significant computing resources. Here, we introduce a universal semi-analytical approach to solve the reflection of dipole-excited SPPs from the edge of a metal film by developing the image dipole method for SPPs. This approach achieves the directional propagation of SPPs through a multielement dipole array formed by a single dipole source and its reflections. Doing so mitigates the challenges in integrating and achieving coherent excitation among independently driven electrical sources. In addition, we provide design parameters for tuning the amplitude and phase of the image dipoles to engineer the directivity of SPP propagation. The configurations discussed can be readily implemented in the setting of tunnel-junction-based plasmon sources.

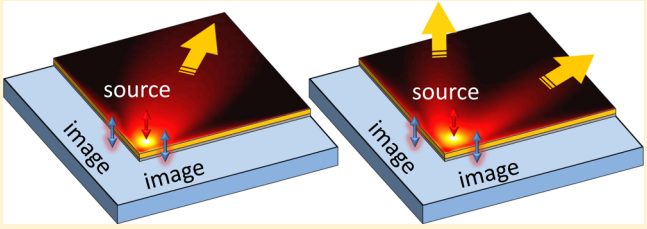

KEYWORDS: *image dipole, surface plasmon polariton, plasmon reflection, dipole, directional propagation*

The tight confinement and guiding of light on metal surfaces in the form of surface plasmon polaritons (SPPs) plays a key role in bridging optics and electronics by shrinking optical elements to the nanoscale[1] and potentially increasing the speed of electronic devices.[2−4] To implement densely integrated optical nanocircuits, we need sources of SPPs that are ultracompact in volume, can be electrically driven, and provide directional emission.[5−7] An example of the most compact electrical source of plasmons is found in the inelastic tunneling of electrons at the tip of a scanning tunneling microscope (STM).[8,9] These sources are pointlike in nature and can be approximated by simple out-of-plane electric dipoles.[10] Albeit inherently inefficient, they nonetheless provide a platform for investigating the directional emission and beaming of plasmons from point sources on nanostructures and adjacent to metal edges.

Directional excitation of SPPs in optical nanocircuits is crucial in controlling energy/information flow to provide complex functionality. Unlike an elliptically polarized dipole, which can excite asymmetric SPPs,[11,12] a simple out-of-plane dipole can only excite cylindrically symmetric SPPs. To break this inherent symmetry and achieve directional emission, we look to the "antenna array" used in radiofrequency (RF) communication, where an array of dipole antennas is used to beam electromagnetic radiation by controlling the relative phase and position of the individual dipoles.[13] Though effective at RF, implementing a dipole array at optical frequencies is impractical, as individual electrical sources of plasmons are incoherent with respect to one another. We instead utilize a single dipole source and its reflections from multiple edges of a metal film to form an "effective" dipole array. Although analytical approaches for the reflection of plane-wave SPPs off metal edges have been developed,[14] the reflections of SPPs excited by dipole sources have not been investigated. For dipole-excited SPPs, existing analytical works only focus on the cases of unbounded metal films,[11,15] and their reflections off edges still rely on full numerical simulations, which are time-consuming. A yet-to-be-developed analytical approach to determine the reflection of SPPs excited by a dipole source will enable rapid determination of the emission profile of SPPs from point sources and its reflections off adjacent geometries.

In this paper, we present a semianalytical method to create multielement dipole arrays for achieving the beaming of SPPs from a single vertically oriented dipole source. We calibrate and compare this method with results from full numerical simulations. The key principle is to rely on the interference of plasmons excited from a single point dipole with its reflection(s) off the edge(s) of a metal film. We show that these

Received: August 31, 2014
Published: November 18, 2014

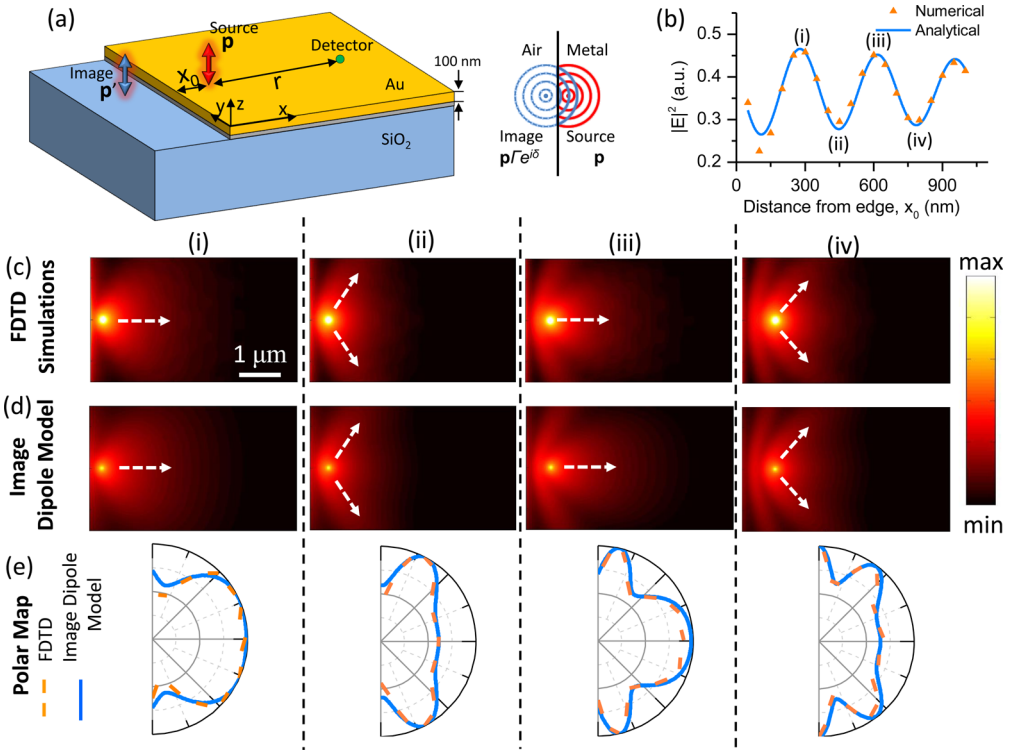

Figure 1. Image dipole model for SPP reflections from the edge of a semi-infinite Au film on a glass substrate. (a) Schematic of the simulation setup. (Inset) SPP wavefronts on the metal film as it originates from a dipole and its image. The source dipole **p** (red) is placed 5 nm above a semi-infinite Au film at (x_0, y_0, z_0). An image dipole **p**′ (blue) at $(-x_0, y_0, z_0)$ with a complex amplitude $\mathbf{p}\Gamma \exp(i\delta)$ is used to model the reflected SPPs. (b) Plot of electric field intensity measured at a distance $r = 3$ μm from the source (green dot in (a)) as a function of the dipole distance from the edge, x_0. The constructive and destructive interference between the SPP and its reflection is seen as oscillations in the plot. The analytical curve shown as the blue solid line was fitted to the numerical data (orange triangles) using $\Gamma = 0.15$ and $\delta = 0.35\pi$. (i–iv) dipole positions at $x_0 = 300$, 450, 600, and 800 nm, respectively, corresponding to the constructive/destructive interferences. The exact distance between a constructive interference point and its neighboring destructive interference point should be one-quarter of the SPP wavelength (λ_{SPP}), which is 169 nm in this case. Since our simulations were performed in steps of 50 nm, (i–iv) were chosen to be the closest available data points. (c) Electric field intensity $|\mathbf{E}|^2$ (1nm above the Au surface) numerically determined from full electromagnetic simulations using a finite-difference time-domain (FDTD) method for the four representative dipole positions depicted in (b), where constructive/destructive interferences occur. (d) Electric field intensity $|\mathbf{E}|^2$ calculated from the analytical image dipole model. (e) Polar map for the SPP radiation patterns (1 nm above metal surface) showing good agreement between numerical and analytical results.

reflections can be conveniently determined using an image dipole, with a well-defined amplitude and phase shift. The introduction of the imaginary dipole, as traditionally used in electrodynamics,[16,17] and some scattering problems,[18] is now extended to the reflection of SPPs, and it enables us to analytically determine the plasmon propagation profile without full electromagnetic simulations. We also show that the reflection coefficient depends on the properties of the edges and gaps in the metal film. These features provide additional degrees of freedom to control the SPP beam. Through the method of images, our design approach can be readily applied to the development of on-chip and position-tunable compact plasmon sources and switches, and single- and/or multi-tip near-field optical microscopy.

We start with the theoretical analysis of SPPs excited by a single out-of-plane dipole $\mathbf{p} = pe^{-i\omega t}\hat{z}$ placed above a flat metal film. The metal–air interface is at the plane $z = 0$, and the dipole source is placed at a height z_0 above the plane. In a cylindrical coordinate system (ρ, ϕ, z) centered at the dipole position, the electric field of the dipole-excited SPP at a distance ρ greater than a few $1/|k_{spp}|$ from the source and measured at a distance d above the metal film can be expressed as[11,19]

$$\mathbf{E} = C\frac{\exp(ik_{SPP}\rho)}{\sqrt{k_{SPP}\rho}}p\vec{v} \tag{1}$$

where $C = 2M(k_{SPP}/k_{z,1})e^{ik_{z,1}z_0}e^{ik_{z,1}d}e^{-i\omega t}$; $k_{SPP} = k_0(\epsilon_1\epsilon_2/(\epsilon_1 + \epsilon_2))^{1/2}$ is the complex SPP propagation constant; $\vec{v} = \hat{\rho} - (k_{SPP}/k_{z,1})\hat{z}$; ϵ_1 and ϵ_2 are the permittivity of the dielectric and metal, respectively; $k_{z,1}$ and $k_{z,2}$ are the SPP wave numbers along the axis $\hat{z}$, calculated as $k_{z,n}^2 = k_0^2\epsilon_n - k_{SPP}^2$; and $M = -0.5[(k_{z,1}k_{z,2})/((2\pi)^{1/2}\epsilon_0)](k_{z,1}\epsilon_2 - k_{z,2}\epsilon_2)e^{-(i\pi/4)}$ is the coupling coefficient. Though a far-field approximation is used here, near-field corrections can be added to calculate the field distribution near the source region. Detailed expressions are given in refs 11 and 19.

As shown in Figure 1(a), the SPP spreading away from the dipole source will be partially reflected from the edge. We observe that the reflected SPP propagates as if it originates from an image dipole, located at an equal distance away from the edge as the original dipole [Figure 1(a) inset and Figure S2]. Therefore, we model the reflection by an image dipole, with its amplitude and phase related to the original dipole by a complex scaling factor as

$$\mathbf{p}' = \mathbf{p}\Gamma \exp(i\delta) \tag{2}$$

dx.doi.org/10.1021/ph500324e | ACS Photonics 2014, 1, 1307–1312

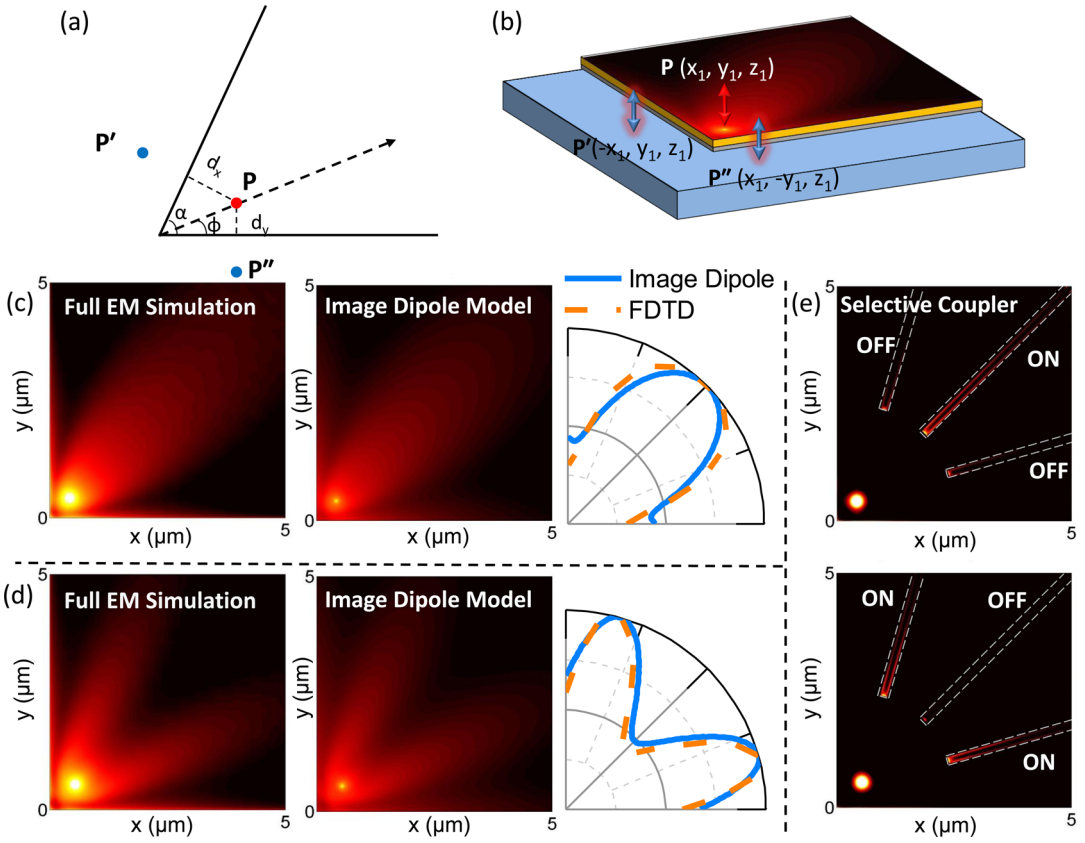

Figure 2. Three-element dipole array formed by placing a dipole near an idealized corner of an Au film. (a) Schematic for placing a dipole near a corner with a generalized angle α. (b) Simulated structure, where the dipole is situated near a right-angle corner. (c) and (d) Intensity distributions for the cases of diagonal and antidiagonal SPP emissions achieved by simply tuning the dipole position from $x_0 = y_0 = 419$ nm to $x_0 = y_0 = 539$ nm. The 1st column and 2nd column present the intensity distributions calculated by FDTD simulation and image dipole model, respectively. The 3rd column presents the polar plot of the radiation patterns. (e) A selective coupler based on the position-tunable directional emission of SPPs, where three slit waveguides are etched into the Au film with a right-angle edge.

where $\mathbf{p}$ is the original dipole and $\mathbf{p}'$ is the image dipole. Γ and δ are the amplitude scaling factor and phase shift of the reflection coefficient, respectively. In principle, the reflection coefficient is angle-dependent, as discussed in Figure S1 and Figure S2.[14] For the sake of simplicity, it is taken as a constant while maintaining good agreement with numerical calculations, as shown later. The validity of the image dipole approach requires that the SPP maintains coherence upon reflection.[20]

To investigate the validity of the image dipole approach, we first set up the general expression for the total electric fields from both the source and the image dipoles. The edge of the metal film is at $x = 0$. With the source dipole located at (x_0, y_0, z_0), the image dipole is formed at $(-x_0, y_0, z_0)$. The total electric field of the SPP on the metal film is the linear superposition of the fields originating from the source and image: $\mathbf{E} = \mathbf{E}_I + \mathbf{E}_S$. For a dipole pair, constructive and destructive interferences would cyclically occur as we vary the distance between the two dipoles. Now, if we observe the electric field intensity using a monitor/detector at $(x_0 + r, y_0, d)$, i.e. at a distance r away from the source dipole, the total electric field intensity is given by

$$|\mathbf{E}|^2 = |\mathbf{E}_S + \mathbf{E}_I|^2 = D\left|1 + \frac{\exp(i2x_0k_{SPP})}{\sqrt{1 + 2x_0/r}}\Gamma e^{i\delta}\right|^2 \quad (3)$$

where $D = |[C \exp(ik_{SPP}r)/(k_{SPP}r)^{1/2}]\vec{p}\vec{v}|^2$, and $k_{SPP} = k'_{SPP} + ik''_{SPP}$. Here, the field is expressed in Cartesian coordinates, with $\vec{v} = \hat{x} - (k_{SPP}/k_{z,1})\hat{Z}$. Two main results can be drawn from eq 3. First, constructive interference occurs when $\delta + 2x_0k'_{SPP} = 2n\pi$, and destructive interference when $\delta + 2x_0k'_{SPP} = (2n + 1)\pi$, where $n = 0, 1, 2, \ldots$. Second, the modulation depth, i.e. the ratio of $|\mathbf{E}|^2$ at maxima and minima, is expressed as

$$\left(\frac{1 + \Gamma \exp(-k''_{SPP}2x_0)/\sqrt{1 + 2x_0/r}}{1 - \Gamma \exp(-k''_{SPP}2x_0)/\sqrt{1 + 2x_0/r}}\right)^2$$

This expression reduces to

$$\left(\frac{1 + \Gamma \exp(-k''_{SPP}2x_0)}{1 - \Gamma \exp(-k''_{SPP}2x_0)}\right)^2$$

for $r \gg x_0$ and approaches unity for large values of x_0. Therefore, one would expect the electric field intensity along the positive x-direction to undergo a cyclic change with decreasing modulation depth (due to propagation losses) as the original dipole moves away from the film edge. This simple expression eventually allows us to characterize the reflection coefficient using full electromagnetic simulations by measuring the intensity dependence on the dipole position.

We performed full electromagnetic simulations using the finite-difference time-domain (FDTD) method to test our model. As shown in Figure 1(a), the simulated structure consists of a 100-nm-thick semi-infinite Au film on top of a glass substrate, with a 20-nm-thick Cr adhesion layer to damp

dx.doi.org/10.1021/ph500324e | ACS Photonics 2014, 1, 1307−1312

out the SPP on the metal−glass interface. An out-of-plane dipole source of 700 nm wavelength is placed at (x_0, y_0, z_0), where $y_0 = 0$, $z_0 = 5$ nm, and x_0 varies from 50 to 1000 nm with a step of 50 nm. The electric field intensity $|\mathbf{E}|^2$ captured at the monitor ($r = 3$ μm and $d = 1$ nm, indicated as a green dot in Figure 1(a)) is denoted as orange triangles in Figure 1(b). This simulation result verifies our prediction that the field intensity experiences a cyclic oscillation with decreasing modulation depth as the dipole moves away from the film edge. We fit the simulation results using the image dipole model in eq 3 [Figure 1(b), blue solid line] using $\Gamma = 0.15$ and $\delta = 0.35\pi$. Note that Γ and δ are only dependent on the structure and independent of the source/observation position. These values accurately match the reflection coefficient of a plane-wave SPP at normal incidence ($\Gamma = 0.14$ and $\delta = 0.34\pi$).[14] In this case, we can approximate the reflection coefficients of dipole-excited SPPs using that of plane-wave SPPs at normal incidence, whose analytical expression is readily available.[14] This approximation will greatly simplify our model. In Figure 1(b), the image dipole model agrees well with the FDTD simulations, except for the region where the dipole is very close to the edge (e.g., $x_0 = 50$−150 nm), because our theoretical treatment only works for the far-field region (from eq 1) and neglects coupling to other local modes.

Next we compared the field distribution and radiation patterns calculated from the numerical simulation (FDTD simulations) and analytical model (image dipole model). Figure 1(c) shows the FDTD simulation results for the electric field intensity patterns at four representative source positions depicted in Figure 1(b), where constructive and destructive interferences occur. As shown in Figure 1(d), the analytical image dipole model captures these field patterns accurately. Figure 1(e) presents the polar plot of the SPPs' Poynting vector at 1 nm above the metal surface. The intensity distribution and radiation pattern from the FDTD simulation and image dipole model show a good quantitative agreement on the emission angle, with an error of less than 0.5°. More comparisons of the field intensity and radiation patterns for different x_0 values with higher-order constructive/destructive interferences are shown in the Supporting Information movie ph500324e_si_002.avi. Note that the field intensity distribution calculated from the FDTD simulations captures not only the field of SPPs but also the direct light emission from the dipole. Therefore, it has a higher intensity around the source region compared to that calculated from the image dipole model, which captures only the SPP fields.

By simple reflection, a two-element dipole array has been formed effectively, and created directional emission of SPPs, but with limited directivity. To increase the directivity for beaming of SPPs, we introduce edges to create more image dipoles, as more elements in an antenna array can yield better directivity.[13] Figure 2(a) shows a generalized case for placing a dipole near a corner with an angle of α, where two image dipoles are created. Directional emission along angle ϕ is achieved when all three dipoles constructively interfere along that direction:

$$k'_{SPP} 2d_y \sin\phi + \delta = 2\pi m \quad \text{and}$$
$$k'_{SPP} 2d_x \sin(\alpha - \phi) + \delta = 2\pi n \tag{4}$$

where m and n are integers. d_x and d_y denote the distances from the dipole to two edges. Similarly, to suppress the emission at the angle ϕ requires the following:

$$k'_{SPP} 2d_y \sin\phi + \delta = 2\pi(m + 0.5) \quad \text{and}$$
$$k'_{SPP} 2d_x \sin(\alpha - \phi) + \delta = 2\pi(n + 0.5) \tag{5}$$

Figure 2(b−d) shows the case of a source dipole near a right-angle corner (i.e., $\alpha = 90°$) on an Au film. Two image dipoles are created because of the two edges. We neglect second-order images induced by the first-order image dipoles, as they are highly attenuated ($\Gamma^2 p \approx 0.02p$). Using the reflection coefficients obtained from the single-edge reflection, and eq 4 and 5, we get $x_0 = y_0 = 419$ nm and $x_0 = y_0 = 539$ nm for diagonal and antidiagonal emissions (i.e., $\phi = 45°$), respectively. As shown in Figure 2(c) and (d), we observe a clear improvement on the directivity compared to the single-edge case, and an excellent agreement between the FDTD simulations and the image dipole model. In such a simple structure, a change of the dipole position can drastically tune the emission direction of the excited SPPs. Based on this configuration, an on-chip and position-tunable selective coupler for SPP can be implemented, as theoretically shown in Figure 2(e) (field pattern captured at 30 nm under the top Au surface), where three 150 nm-wide slit waveguides are introduced. When the dipole source is placed at $x_0 = y_0 = 419$ nm (upper panel), the diagonal waveguide along 45° is switched "ON"; and when the dipole source is shifted to $x_0 = y_0 = 539$ nm (lower panel), the off-diagonal (16° and 74°) waveguides are switched "ON". The performance of the simple selective coupler can be improved by modifying the angle of the corner, i.e. to match the null in one case to the maxima in the other case, and the design of the waveguide, e.g. slit width, depth, direction, and position.

We take a step further to introduce more edges near the source dipole to create more image dipoles, and therefore form multielement dipole arrays. Figure 3(a−c) presents the case for three edges, with parameters optimized for directional emission along the x-direction. The distance between the dipole and the middle edge is 279 nm (derived from the case of single-edge reflection); and the distance between the dipole and the upper and lower edge is 419 nm (adopted from the case of 2-edge reflection). Note that $\Gamma = 0.15$ and $\delta = 0.35\pi$ are still valid and provide good accuracy.

In the limiting case, where the number of edges approaches infinity, we effectively form a curved edge. A special and interesting case is to employ a parabolic curve to mimic a parabolic mirror for SPPs. It can be mathematically proven that when a dipole source is put at the focal point, it will create an infinite number of image dipoles that line up along a straight line, as shown in Figure 3(d) (see Figure S3 for derivation). According to Huygens' Principle, the SPP wavefront emitted by this straight line of dipoles will be like a plane wave (see Figure S4 for the wavefront of the reflected SPP). As a result, the SPP reflection over a parabolic edge is essentially the superposition of a "plane-wave SPP" and a point-excited SPP, as shown in Figure 3(d−f). Again, we design the focal point to be 279 nm away from the vertex for the parabolic curve to enhance the directional emission to positive x-direction. In Figure 3(f), we assume that the plane-wave SPP has an amplitude of $C \times 0.15p$ (see eq 1) and phase of 0.35π at $x = -279$ nm, based on the image dipole characteristic that $\Gamma = 0.15$ and $\delta = 0.35\pi$.

In addition to changing the number of edges, the directional emission can be further controlled by engineering the reflection coefficient, which depends on the edge properties. Using the method in Figure 1, we calculated the reflection coefficients for

dx.doi.org/10.1021/ph500324e | ACS Photonics 2014, 1, 1307−1312

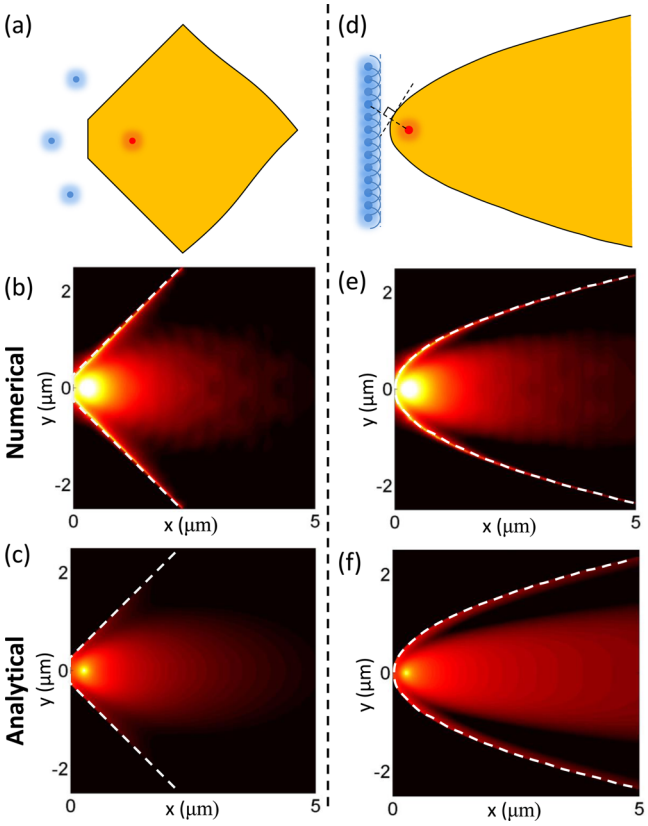

Figure 3. Extending image dipole model to multiple and continuous edges. (a–c) Putting three edges near a dipole creates three image dipoles and forms a four-element array. (d–f) Infinite number of image dipoles created when the source dipole is placed near a parabolic edge. (b) and (e) are the electric field intensity from FDTD simulations. (c) and (f) are from image dipole models.

two other common plasmonic materials: aluminum ($\Gamma = 0.12$ and $\delta = 0.30\pi$) and silver ($\Gamma = 0.14$ and $\delta = 0.33\pi$), yielding remarkably similar values. We also show that the reflection coefficient is insensitive to the radius-of-curvature of the edge (<1% in amplitude Γ and 0.02π in phase shift δ for 10 nm change in the radius-of-curvature) [Figure S5(a) and (b)]. This analysis indicates a reasonable tolerance to fabrication imperfections. On the other hand, adding neighboring metal films near the edge can modify the reflection coefficient significantly (modulation range for Γ is ~0.2 and that for δ is ~0.6π) and, therefore, enables one to tune the strengths of the image dipoles [Figure S5(c) and (d)]. This extra degree-of-freedom for engineering the reflection coefficient can be utilized to improve the directionality of SPP emissions, as shown in Figure 4. In Figure 4(b), neighboring gold films are added, with a gap size of 200 nm, giving maximum reflectivity as shown in Figure S5(d). Based on this new reflection coefficient ($\Gamma = 0.24$, $\delta = 0.29\pi$), from eq 4, we obtained $x_0 = y_0 = 410$ nm for diagonal emission. Figure 4(c) shows the SPP radiation pattern extracted from FDTD simulations, where a clear improvement of directivity is observed. Note that the polar map is normalized.

The image dipole method that we developed is a general approach for analytically determining the reflection of SPPs from edges in a variety of metals and edge geometries. This method allows SPPs from a single dipole source to be beamed due to reflections from edges on metal films. Through bypassing the calculation of complex physical processes involved in plasmon reflection, e.g. the formation of surface charges along the edges, it enables the analytical prediction of dipole-excited SPPs near metal film edges. Although we have focused only on out-of-plane dipoles, we expect similar treatments for in-plane dipoles. The configurations discussed can be readily implemented using tunnel-junction-based plasmon emitters, e.g. STM, and other point sources of plasmons, such as focused electron beams and quantum emitters. This simple model and design approach directly facilitate the development of position-tunable compact plasmon sources for optical nanocircuits, and they simplify calculations of SPPs from multiple scatterers.

METHODS

Finite-Difference Time-Domain (FDTD) simulations were performed using the commercial software Lumerical FDTD Solutions. In the simulations, the free-space wavelength of the dipole source was 700 nm. The permittivity of Cr and Au used were $\epsilon_{Cr} = -4.36 + 33.55i$ and $\epsilon_{Au} = -15.71 + 1.28i$.[21] The simulation domain was enclosed by perfectly matched layers (PML). The polar maps of the radiation patterns were plotted by projecting the SPPs' Poynting vector along the radial direction on a semicircle with a radius of 2 μm centered at the source dipole. The Poynting vector $\mathbf{S}$ is calculated as $\mathbf{S}(\varphi) = \mathbf{E} \times \mathbf{H}^*$, where $\mathbf{H}$ is the magnetic field and φ denotes the azimuthal angle. The projection of the Poynting vector along the radial direction was calculated using $\vec{\rho}\cdot\mathbf{S}(\varphi)$, where $\vec{\rho}$ denotes the radial vector pointing away from the source dipole.

ASSOCIATED CONTENT

Supporting Information

Analysis of the angle-dependent reflection coefficient, illustration of SPP reflection over parabolic edges, image dipoles formed in a parabolic mirror, wavefront for the SPP reflected from a parabolic edge, engineering the SPP reflection coefficients using the edge properties, and a movie showing the comparison of higher order constructive/destructive

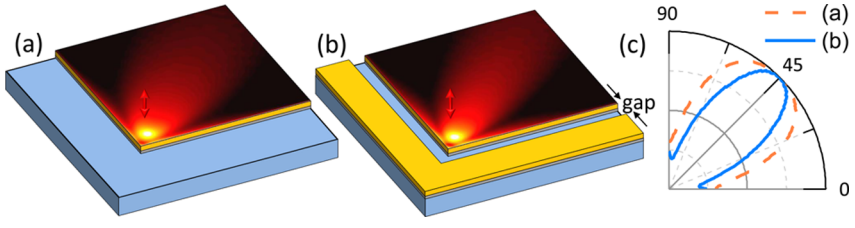

Figure 4. Improving directivity by adding neighboring metal films. (a) Diagonal emission by an unmodified Au corner. (b) Diagonal emission by an Au corner with adjacent Au films, with a gap size of 200 nm. (c) SPP radiation pattern (1 nm above Au surface) obtained from FDTD simulations. With an engineered reflection coefficient, a clear improvement of directivity can be observed.

dx.doi.org/10.1021/ph500324e | ACS Photonics 2014, 1, 1307–1312

reflections over a single edge. This material is available free of charge via the Internet at http://pubs.acs.org.

AUTHOR INFORMATION

Corresponding Author

* E-mail: joel_yang@sutd.edu.sg.

Present Address

[⊥](D.Z.) Department of Electrical Engineering and Computer Science, Massachusetts Institute of Technology, 77 Massachusetts Avenue, Cambridge, Massachusetts 02139, USA.

Author Contributions

[†]D.Z. and Z.D. contributed equally to this work.

Notes

The authors declare no competing financial interest.

ACKNOWLEDGMENTS

We would like to acknowledge the funding support from the Agency for Science, Technology and Research (A*STAR) Young Investigatorship (grant number 0926030138), SERC (grant number 092154099), and National Research Foundation (grant number NRF-CRP 8-2011-07). Also, we thank the A*STAR Computational Resource Centre for the use of computing facilities. J.K.W.Y. thanks Ying Min Wang and Christian A. Nijhuis for fruitful discussions.

REFERENCES

(1) Yu, N.; Genevet, P.; Kats, M. A.; Aieta, F.; Tetienne, J. P.; Capasso, F.; Gaburro, Z. Light propagation with phase discontinuities: generalized laws of reflection and refraction. *Science* **2011**, *334*, 333−7.

(2) Tan, S. F.; Wu, L.; Yang, J. K. W.; Bai, P.; Bosman, M.; Nijhuis, C. A. Quantum Plasmon Resonances Controlled by Molecular Tunnel Junctions. *Science* **2014**, *343*, 1496−1499.

(3) Engheta, N. Circuits with light at nanoscales: optical nanocircuits inspired by metamaterials. *Science* **2007**, *317*, 1698−702.

(4) Staffaroni, M.; Conway, J.; Vedantam, S.; Tang, J.; Yablonovitch, E. Circuit analysis in metal-optics. *Photonics Nanostruct.* **2012**, *10*, 166−176.

(5) Falk, A. L.; Koppens, F. H. L.; Yu, C. L.; Kang, K.; de Leon Snapp, N.; Akimov, A. V.; Jo, M.-H.; Lukin, M. D.; Park, H. Near-field electrical detection of optical plasmons and single-plasmon sources. *Nat. Phys.* **2009**, *5*, 475−479.

(6) Huang, K. C. Y.; Seo, M.-K.; Sarmiento, T.; Huo, Y.; Harris, J. S.; Brongersma, M. L. Electrically driven subwavelength optical nanocircuits. *Nat. Photonics* **2014**, *8*, 244−249.

(7) Walters, R. J.; van Loon, R. V. A.; Brunets, I.; Schmitz, J.; Polman, A. A silicon-based electrical source of surface plasmon polaritons. *Nat. Mater.* **2010**, *9*, 21−25.

(8) Bharadwaj, P.; Bouhelier, A.; Novotny, L. Electrical Excitation of Surface Plasmons. *Phys. Rev. Lett.* **2011**, *106*, 226802.

(9) Wang, T.; Boer-Duchemin, E.; Zhang, Y.; Comtet, G.; Dujardin, G. Excitation of propagating surface plasmons with a scanning tunnelling microscope. *Nanotechnology* **2011**, *22*, 175201.

(10) Marty, R.; Girard, C.; Arbouet, A.; Colas des Francs, G. Near-field coupling of a point-like dipolar source with a thin metallic film: Implication for STM plasmon excitations. *Chem. Phys. Lett.* **2012**, *532*, 100−105.

(11) Mueller, J. P. B.; Capasso, F. Asymmetric surface plasmon polariton emission by a dipole emitter near a metal surface. *Phys. Rev. B* **2013**, *88*.

(12) Rodriguez-Fortuno, F. J.; Marino, G.; Ginzburg, P.; O'Connor, D.; Martinez, A.; Wurtz, G. A.; Zayats, A. V. Near-Field Interference for the Unidirectional Excitation of Electromagnetic Guided Modes. *Science* **2013**, *340*, 328−330.

(13) Hansen, R. C. *Phased Array Antennas*; Wiley: 2009.

(14) Gordon, R. Vectorial method for calculating the Fresnel reflection of surface plasmon polaritons. *Phys. Rev. B* **2006**, *74*, 153417.

(15) Hecht, B.; Bielefeldt, H.; Novotny, L.; Inouye, Y.; Pohl, D. W. Local Excitation, Scattering, and Interference of Surface Plasmons. *Phys. Rev. Lett.* **1996**, *77*, 1889−1892.

(16) Jackson, J. D. *Classical electrodynamics*, 3rd ed.; Wiley: New York, 1999; pp xxi, 808.

(17) Novotny, L.; Hecht, B. *Principles of Nano-Optics*; Cambridge University Press: 2006.

(18) Mollet, O.; Bachelier, G.; Genet, C.; Huant, S.; Drezet, A. Plasmonic interferometry: Probing launching dipoles in scanning-probe plasmonics. *J. Appl. Phys.* **2014**, *115*, 093105.

(19) Archambault, A.; Teperik, T. V.; Marquier, F.; Greffet, J. J. Surface plasmon Fourier optics. *Phys. Rev. B* **2009**, *79*.

(20) Dong, Z.; Chu, H.-S.; Zhu, D.; Du, W.; Akimov, Y. A.; Goh, W. P.; Wang, T.; Goh, K. E. J.; Troadec, C.; Nijhuis, C. A.; Yang, J. K. W. *Electrically-excited surface plasmon polaritons with directionality control.* submitted.

(21) Palik, E. D. *Handbook of Optical Constants of Solids*; Academic Press: 1998.